NUMERICAL SIMULATION OF 1993 SOUTHWEST HOKKAIDO EARTHQUAKE TSUNAMI AROUND OKUSHIRI ISLAND

By Shinji Sato[1]

ABSTRACT: This paper reports a numerical simulation of tsunami propagation for the 1993 Southwest Hokkaido earthquake tsunami. The model is based on the Boussinesq equation, which includes the effects of frequency dispersion. Energy dissipation due to breaking at the tsunami wave front is modeled. The validity of the model was tested with the existing laboratory data of dispersive wave trains breaking on a slope. The model was then applied to the simulation of the 1993 Southwest Hokkaido earthquake tsunami around the southern part of Okushiri Island. Comparison with the physical model demonstrates that it is the dispersion of the wave front which caused focusing of the wave energy at the narrow region on the lee side of the island, consequently increasing the tsunami height.

INTRODUCTION

A large earthquake shook northern Japan at 22:17 on July 12, 1993, Japan Standard Time, and generated huge tsunamis which caused devastating damage mainly on Okushiri Island. This earthquake was named the 1993 Southwest Hokkaido earthquake; the epicenter was close to Okushiri Island. The sea bottom displacements that generated the tsunamis are located in the region west of Okushiri Island. The first tsunami attacked the island from the west as early as 5 min after the origin time. At Cape Aonae, located at the southernmost edge of the island (see Fig. 1), a part of the district was flushed over by the first tsunami. The complex bottom topography near Cape Aonae, such as the Okushiri Spur, was considered to be responsible for the peculiar transformation of the tsunami. The complex behavior of the tsunami, such as dispersion and breaking of the tsunami front, may affect the distribution of inundation heights of the tsunami. Although eye witnesses of the tsunami were scarce since the earthquake occurred at night, the field survey reported that the inundation heights were anomalously large at Hamatsumae, located about 2 km northeast of Cape Aonae [Fig. 2; Hokkaido Tsunami Survey Group (1993)]. As shown in Fig. 2, the town of Hamatsumae is located on the lee side of the tsunami source, hence it is difficult to explain the more than 20-m runup height.

The propagation of the tsunami was numerically simulated by many researchers [e.g., Takahashi et al. (1994), Yamashita et al. (1994), Kato and Tsuji (1994)]. However, the anomalously large inundation height at Hamatsumae cannot be adequately explained by the models based on nonlinear nondispersive long-wave equation (shallow-water equation). In this study, a numerical simulation was performed by a model based on the Boussinesq equation. The model simulated the propagation of the tsunami, including the effect of dispersion and the breaking of the tsunami front. The validity of the model was confirmed with the existing laboratory data and inundation heights surveyed on Okushiri Island.

NUMERICAL MODEL

Basic Equations

Numerical computations were carried out by using the nonlinear dispersive wave model proposed by Sato and Kabiling (1994), which includes turbulence effects due to wave breaking. The turbulence effects are modeled by the "eddy-viscosity" model. The basic equations are expressed as follows: the conservation of mass

$$\frac{\partial \eta}{\partial t} + \frac{\partial Q_x}{\partial x} + \frac{\partial Q_y}{\partial y} = 0 \tag{1}$$

the conservation of linear momentum in the x-direction

$$\frac{\partial Q_x}{\partial t} + \frac{\partial}{\partial x}\left(\frac{Q_x^2}{d}\right) + \frac{\partial}{\partial y}\left(\frac{Q_x Q_y}{d}\right) + gd\frac{\partial \eta}{\partial x} = \frac{1}{3}h^2\left(\frac{\partial^3 Q_x}{\partial x^2 \partial t} + \frac{\partial^3 Q_y}{\partial x \partial y \partial t}\right) - \frac{gn^2}{d^{7/3}} Q_x \sqrt{Q_x^2 + Q_y^2} + \nu_e\left(\frac{\partial^2 Q_x}{\partial x^2} + \frac{\partial^2 Q_x}{\partial y^2}\right) \tag{2}$$

the conservation of linear momentum in the y-direction

$$\frac{\partial Q_y}{\partial t} + \frac{\partial}{\partial x}\left(\frac{Q_x Q_y}{d}\right) + \frac{\partial}{\partial y}\left(\frac{Q_y^2}{d}\right) + gd\frac{\partial \eta}{\partial y} = \frac{1}{3}h^2\left(\frac{\partial^2 Q_x}{\partial x \partial y \partial t} + \frac{\partial^3 Q_y}{\partial y^2 \partial t}\right) - \frac{gn^2}{d^{7/3}} Q_y \sqrt{Q_x^2 + Q_y^2} + \nu_e\left(\frac{\partial^2 Q_y}{\partial x^2} + \frac{\partial^2 Q_y}{\partial y^2}\right) \tag{3}$$

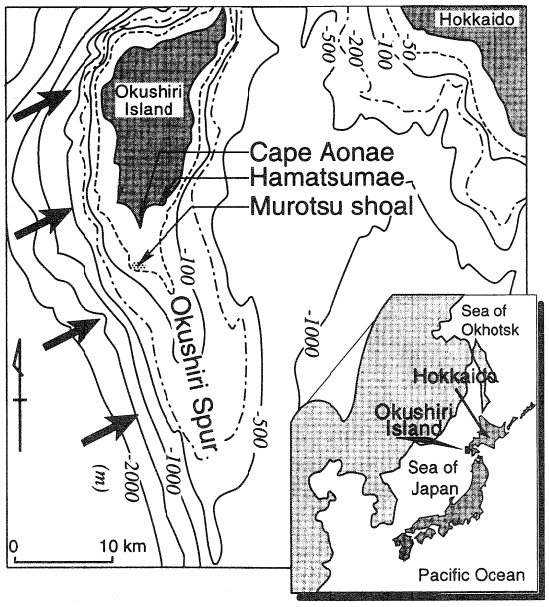

FIG. 1. Sea Bottom Contours around Okushiri Island (Arrow Marks on Left Side Indicate Approximate Tsunami Attack Directions)

[1]Sr. Res., Coast. Engrg. Div., Public Works Res. Inst., 1 Asahi, Tsukuba, 305 Japan.

Note. Discussion open until March 1, 1997. To extend the closing date one month, a written request must be filed with the ASCE Manager of Journals. The manuscript for this paper was submitted for review and possible publication on March 23, 1995. This paper is part of the ***Journal of Waterway, Port, Coastal, and Ocean Engineering***, Vol. 122, No. 5, September/October, 1996. ©ASCE, ISSN 0733-950X/96/0005-0209–0215/$4.00 + $.50 per page. Paper No. 10401.

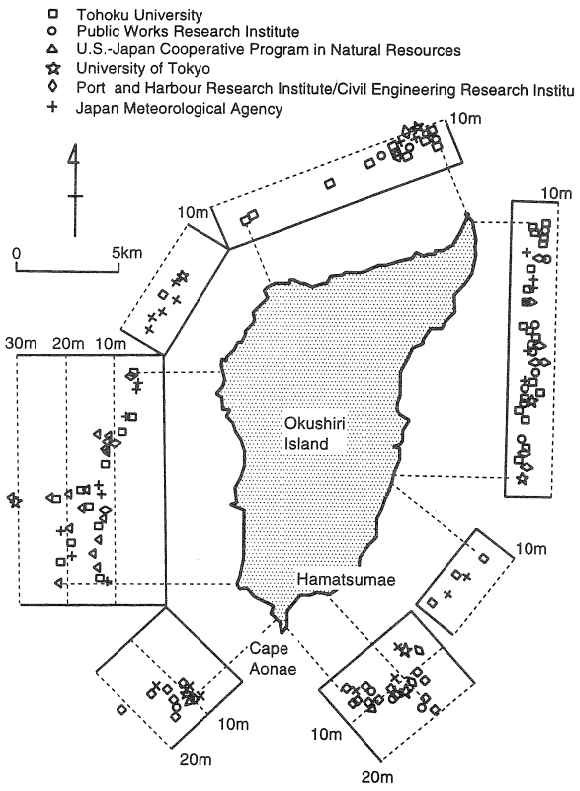

FIG. 2. Distribution of Tsunami Runup Heights measured by Several Survey Groups [Hokkaido Tsunami Survey Group (1993)]

where η = surface elevation; Q_x and Q_y = flow rates in x- and y-directions, respectively; h = water depth; d = $(=h + \eta)$ total depth; n $(=0.026\ \text{m}^{-1/3}\ \text{s})$ = Manning roughness parameter; g = gravity acceleration; and ν_e = eddy viscosity.

The dispersion terms were transformed by using (1) as

$$\frac{1}{3}h^2\left(\frac{\partial^3 Q_x}{\partial x^2 \partial t} + \frac{\partial^3 Q_y}{\partial x \partial y \partial t}\right) = -\frac{1}{3}h^2\frac{\partial^3 \eta}{\partial x \partial t^2}, \quad (4)$$

$$\frac{1}{3}h^2\left(\frac{\partial^3 Q_x}{\partial x \partial y \partial t} + \frac{\partial^3 Q_y}{\partial y^2 \partial t}\right) = -\frac{1}{3}h^2\frac{\partial^3 \eta}{\partial y \partial t^2}. \quad (5)$$

which were discretized by central differences. An efficient alternating directional implicit (ADI) scheme proposed by Maa (1990) was used in the numerical integration. The ADI scheme, compared with the explicit leap-frog scheme, which introduces upwind finite difference in the discretization of the advection term, has the advantage of achieving efficient and stable computation without losing accuracy. The variables η, Q_x, and Q_y were arranged in a horizontally staggered two-dimensional mesh, and the spatial derivatives in (1)–(3) were replaced by central differences. The variables η and Q_x at the next time step were implicitly solved from (1) and (2). The variables η and Q_y were then solved from (1) and (3). The details of the algorithm were described in Maa (1990), although the dispersion term was not included in his formulation. The land boundaries were set along the line where the still-water depth was zero, at which waves were assumed to be fully reflective. The surface elevation of the incident wave was specified at the incident boundary.

Momentum Mixing due to Wave Breaking

During the 1983 Central Japan Sea earthquake tsunami, dispersion and breaking of the offshore wave fronts were observed (Shuto 1985). In laboratory experiments of the 1993 Southwest Hokkaido earthquake tsunami, Noguchi et al. (1995) reported that shoaled tsunami experienced breaking in the shallow sea. To compute tsunami transformation, including wave breaking, an appropriate estimation of the breaking point and the associated eddy viscosity ν_e must be estimated.

Sato and Kabiling (1994) proposed a numerical model of monochromatic wave transformation in the surf zone based on the Boussinesq equations. The wave-breaking criterion was set empirically such that waves start breaking when the ratio of the water particle velocity u_s at the crest surface to the wave celerity C exceeded a critical value (0.4–0.6). The use of the ratio u_s/C as the breaking criterion is reasonable since it was based on the physical process of wave breaking and was successfully applied to the breaking of compound wave trains by Watanabe et al. (1984). Sato and Kabiling (1994) computed the eddy viscosity in the surf zone in terms of the energy dissipation coefficient introduced by Watanabe and Dibajnia (1988). The same approach is used in this study with the following modifications.

The critical value of u_s/C for the incipient wave breaking was determined to be 0.4 on the basis of comparison with the laboratory measurements explained later. The water particle velocity u_s at the surface was estimated from the Boussinesq theory in which the vertical profile of the horizontal component of water particle velocity was assumed to be parabolic. The wave celerity C was determined by

$$C = \sqrt{g(h + \eta)} \quad (6)$$

which is considered to be a good approximation in shallow water.

The eddy viscosity model by Sato and Kabiling (1994) was formulated for periodic waves. In their model, the spatial distribution of eddy viscosity in the surf zone was estimated on the basis of the computed wave field. Although this approach was verified for a wide range of laboratory data, it cannot be directly applied to the tsunami since the transformation of the tsunami is transient. To simulate momentum mixing due to tsunami breaking in a simple manner, the eddy viscosity was assumed to be constant in this study in an area shallower than the instantaneous breaking point determined from the u_s/C criterion. Since the breaking phenomenon in shallow water is characterized by the water depth at the breaking point, the velocity scale of the breaking-induced turbulence is estimated by the wave celerity at the breaking point. The dimensional argument leads to the following formulation of eddy viscosity:

$$\nu_e = \alpha\sqrt{gh_{b\max}}\cdot h_{b\max} \quad (7)$$

where $h_{b\max}$ = largest depth of incipient wave breaking, and α = a nondimensional coefficient to be calibrated by comparison with existing data of breaking tsunami transformation. The value of ν_e was determined by (7) in the area shallower than $h_{b\max}$ and set at the molecular viscosity of water elsewhere.

The numerical model presented in this study is first verified with the existing laboratory data for a uniform slope in order to demonstrate its capability of modeling frequency dispersion effects. Then, the model is applied to tsunami simulation around Okushiri Island. The simulated tsunami is compared with the 1/1,100 scale laboratory model results as well as the field runup measurements. Goto (1984) reported that, on the basis of numerical simulation of tsunami based on the Boussinesq equation, dispersion terms should be included in the area shallower than 30 m and the grid size should be smaller than 10 m in prototype scales. In this simulation, therefore, the dispersion terms should be included in the area shallower than 3 cm and the grid size should be smaller than 1 cm. In the present computations, the dispersion terms were actually included in the area shallower than 15 cm. The smallest grid

of 2 cm was used in all the computations, which was the smallest grid size limited by available computer resources.

COMPARISON WITH 1D (UNIFORM SLOPE) PHYSICAL MODEL

Tsuruya et al. (1984) performed a series of experiments, in a 163 m long and 1 m wide wave flume, to investigate the transformation of dispersive wave trains breaking on a gently sloping bottom. Results of the present numerical model were compared with the measurements for a long wave with a period of 40 s on a 1/200 slope. The leading wave started from a rise in water level. The computations were carried out in a narrow domain, 100 m long and 10 cm wide. The shore boundary was set at the still-water shoreline where the normal flux was assumed to be zero. The incident boundary was set at the depth of 50 cm. The experimental data indicate that the water-surface profile at the incident boundary was well approximated by a sinusoidal wave. A sinusoidal wave was therefore used as the input to the numerical model. Although the incident wave was sinusoidal, the shoaled wave on the slope was observed to start to disperse and break. Water-surface elevations in shallow water simulated by the numerical model were compared with those measured at various stations shown in Fig. 3. The comparison was carried out mainly for the condition of incident wave steepness $H_o/L_o = 1.92 \times 10^{-4}$, where H_o is the equivalent deep-water wave height and L_o the deep-water wavelength.

Fig. 4 shows water-surface elevations measured and simulated at station C. Tsuruya et al. (1984) reported that waves at station C were dispersed but not broken. The computational time step Δt was varied from $\Delta t = 0.02$ s to $\Delta t = 0.005$ s. The time t in the computations was the time elapsed from the initiation of sinusoidal wave input at the incident boundary, which did not correspond to the time in experiments since the reference time was not specified in Tsuruya et al. (1984). In the experiment, the wave front was dispersed into two waves at this station with the height of the first wave being about 1.8 cm. In the computations, dispersion into two waves was simulated with time steps $\Delta t = 0.01$ s and $\Delta t = 0.005$ s. The wave heights of the dispersed wave tended to increase with the decrease in time step, although they were underestimated even with $\Delta t = 0.005$ s. Since a significant difference is not noticed in the results of $\Delta t = 0.01$ s and $\Delta t = 0.005$ s, the time step of $\Delta t = 0.01$ s was used in the following computations.

Figs. 5(a) and 5(b) show measured and computed surface elevations at Station C for various wave steepnesses. The dispersion of the wave front was more pronounced and the height of each wave was larger as the incident wave steepness increased. The broken line in Fig. 5(b) shows surface elevation computed by the nondispersive shallow-water theory. It is evident in Fig. 5 that the measured wave fronts are modeled well with the Boussinesq model, although it tends to underestimate the height of each wave in the dispersed wave trains. The computation with shallow-water theory failed to simulate the multiple wave formation at the front.

According to Tsuruya et al. (1984), wave breaking for $H_o/L_o = 1.92 \times 10^{-4}$ occurred between stations C and B. Wave heights in the dispersed wave train were gradually decreased as they approached the shoreline. The value of α in (7) was determined by the comparison of measured and simulated wave profiles. Wave profiles at Station S were compared in Fig. 6 for $\alpha = 0.3$ and $\alpha = 3$. In the experiment, no dispersed waves were observed at Station S, since they were dissipated due to breaking before arriving at Station S. Computed wave profiles at Station S show an abrupt rise in the water level

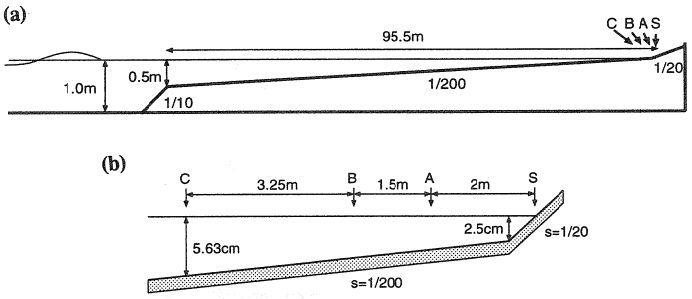

FIG. 3. Experimental setup of Tsuruya et al. (1984): (a) General View; (b) Local View near Shoreline (The Tank is 163 m Long and 1 m Wide, and a Long Wave with 40 s Wave Period was Generated at 140 m from Point C)

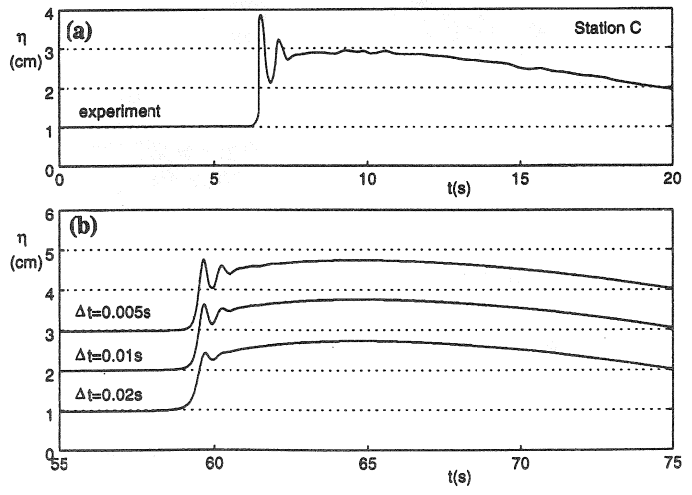

FIG. 4. Comparisons of Wave Profiles at Station C (See Fig. 3): (a) Experimental Data from Tsuruya et al. (1984); (b) Numerical Predictions with Variety of Time Increments

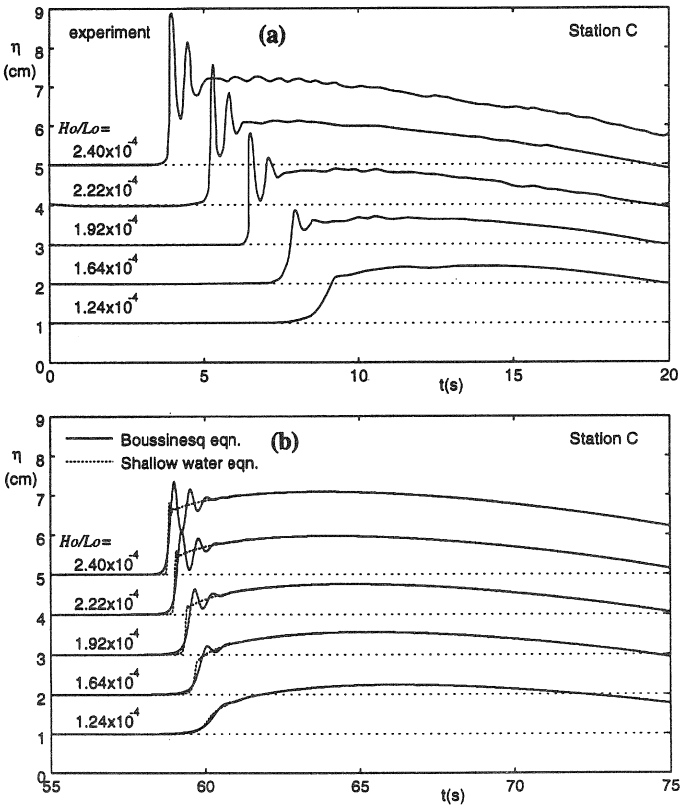

FIG. 5. Comparisons of Wave Profiles at Station C for Various Offshore Wave Steepness H_o/L_o: (a) Experimental Data from Tsuruya et al. (1984); (b) Numerical Predictions Based on Boussinesq Equation ———, and Shallow-Water Equation – – – –

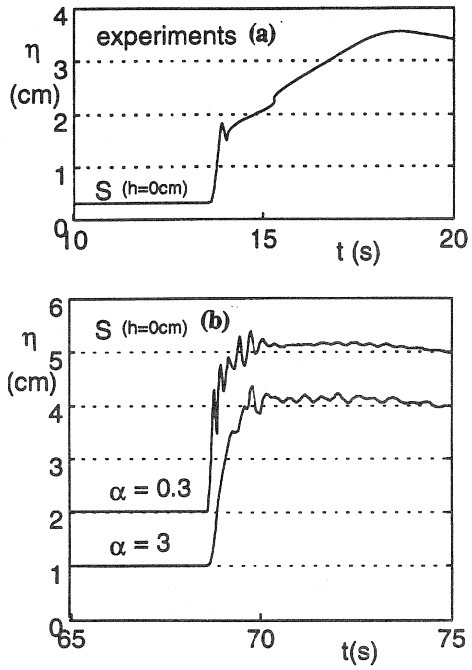

FIG. 6. Wave Profiles at Initial Shoreline: (a) Experimental Data from Tsuruya et al. (1984); (b) Numerical Predictions Based on Boussinesq Equation, Where α is Eddy Viscosity Coefficient in Eq. (7)

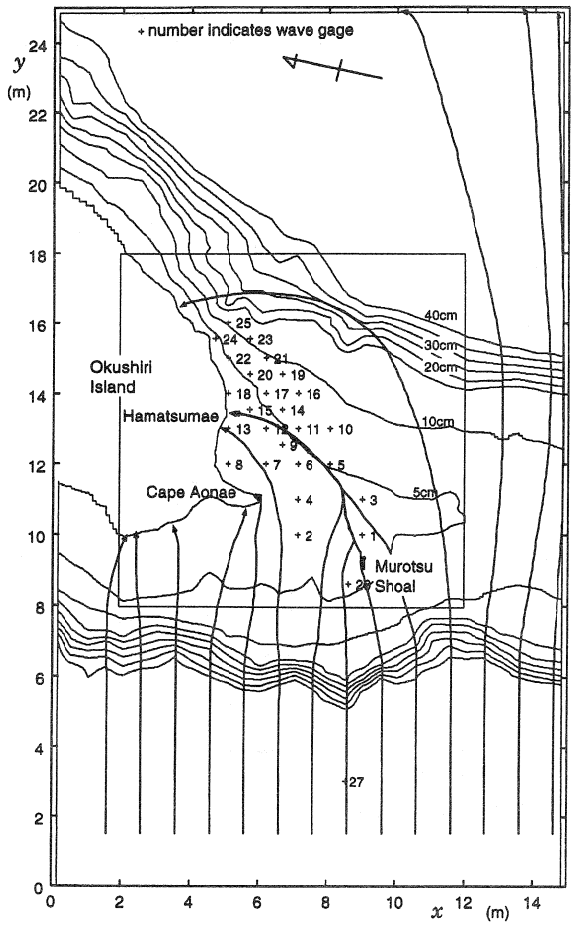

FIG. 7. Computational Domain (Symbol + Identifies Wave Gauge Locations; Line with Arrow Indicates Computed Ray Trajectory of Tsunami Showing Focusing Effect near Hamatsumae, and Caustics Behind Murotsu Shoal)

since the wave runup is not simulated in the model. For α = 0.3, dispersed waves were noticed at Station S while wave dispersions were less significant for α = 3. As further increase in α tended to make the computation unstable, the optimum value of α was determined to be 3.

TRANSFORMATION OF TSUNAMI NEAR OKUSHIRI ISLAND

Noguchi et al. (1995) performed a physical model test which investigated the transformation of the Southwest Hokkaido earthquake tsunami around Cape Aonae using a 1/1,100 nondistorted model in a 30 × 35 m wave basin. The tsunami was generated with a pneumatic wave generator which suctioned the air and lifted the water surface in a chamber prior to the experiment, and by abruptly releasing air through valves attached to the chamber, the water mass in the chamber is released, which created the tsunami in the basin. Since the wall surrounding the basin was highly reflective, the basin was soon disturbed by the reflected waves from the walls. The first wave observed in the basin was not affected by the reflection disturbances. The propagation of the first wave was recorded by video cameras and wave gauges situated mainly on the lee side of Cape Aonae. The computational domain was determined as a 15 × 25 m rectangular region as shown in Fig. 7, which contained the southern part of the source region that was considered to affect the tsunami transformation around Cape Aonae. Computation was carried out and compared with experiments for a 4 mm wave height incidence since it corresponded with the initial water-level rise in the source area (Takahashi et al. 1994).

Fig. 7 illustrates the computational domain and the arrange-

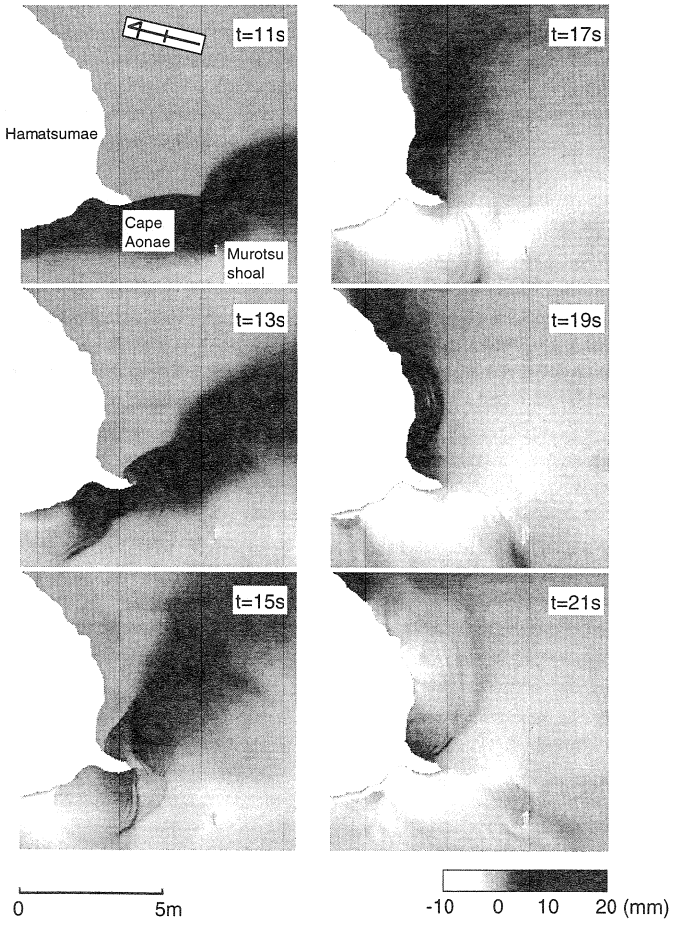

FIG. 8. Propagation of Tsunami around Southern Part of Okushiri Island; Wave Caustics and Dispersion Effects are Shown in Figs. at t = 11 s and t = 13 s

ment of wave gauges in the experiments. Water depth around the island was reproduced from navigation charts published by the Maritime Safety Agency. It is noticed that the Okushiri Spur extends from Cape Aonae and that part of the Murotsu Shoal located on the Spur is above the sea level. The grid sizes were 2 cm in the 10 × 10 m square region shown in Fig. 7 and 10 cm elsewhere. The total number of grids was 550 × 650. The boundary around the island was set at the actual shoreline where normal flux was assumed to be zero in the computation. The minimum depth of the computational grid was 1 mm, which was scaled to be 1.1 m in the prototype. The time step was selected as 0.01 s so that the computation could be carried out with sufficient accuracy. The maximum Courant number, $\sqrt{g(h + \eta)}\Delta t/\Delta x$, was below unity. The incident wave profile was determined from the record of wave gauge No. 27, which was located in front of the wave generator.

Fig. 8 shows the propagation of tsunami simulated by the present Boussinesq model without wave breaking. The symbol t denotes the time elapsed from the initiation of the computation. The surface elevation becomes high at $t = 11$ s in front of Cape Aonae. The first tsunami seemed to have attacked the lowland of Cape Aonae from the bottom (west) at this moment, although it was not simulated in the model since the inundation was not allowed in the computation. At this moment, the offshore waves which were focused behind the Murotsu shoal began to be split into several short waves. The wave rays were curved behind the Murotsu shoal and reached Hamatsumae, located to the east of Aonae, at $t = 17$ s. The waves were then reflected from Hamatsumae, forming a cylindrical wave, and attacked the Aonae district again from the east at $t = 19$ s. The second attack occurred 8 s after the first wave attack, which was 4.5 min in the prototype scale. The actual propagation of the tsunami was also affected by waves coming from the north of the island since the source area was large compared to the island (tsunamis from the north were not modeled in this study). The initial tsunami profile in the source area may also affect the tsunami transformation. It was confirmed however that the dispersion effects of the tsunami front tend to enhance the tsunami height at Hamatsumae as well as the height of waves reflected from Hamatsumae which attacked Aonae again from the opposite direction.

Fig. 9 shows a comparison of temporal wave profiles along the coast. The number denotes the wave gauge number shown in Fig. 7. The left side shows measurements and the right side shows numerical computations. Results of the numerical model simulate dispersion of the wave front at wave gauges No. 8, 13, and 18, which generally agree well with experiments. However, the wave heights of dispersed waves at the tsunami front (indicated in Fig. 9) are underestimated in the numerical model. The difference may be due to the nonlinear transformation of the tsunami in very shallow water since the Boussinesq theory is valid only for weakly nonlinear and weakly dispersive waves.

Fig. 10 shows comparisons of maximum surface elevations along the coastline on the lee side of Cape Aonae. The horizontal axis is the y-coordinate shown in Fig. 7. In the physical model, Cape Aonae is located at $y = 11$ m and Hamatsumae is at $y = 14$ m. Fig. 10(a) indicates the maximum surface elevation simulated by the Boussinesq equation. To compare the numerical results with field measurements, the numerically predicted values are scaled based on the Froude law. Fig. 10(b) shows computation based on shallow-water equation without wave breaking. It is apparent from both figures that the nu-

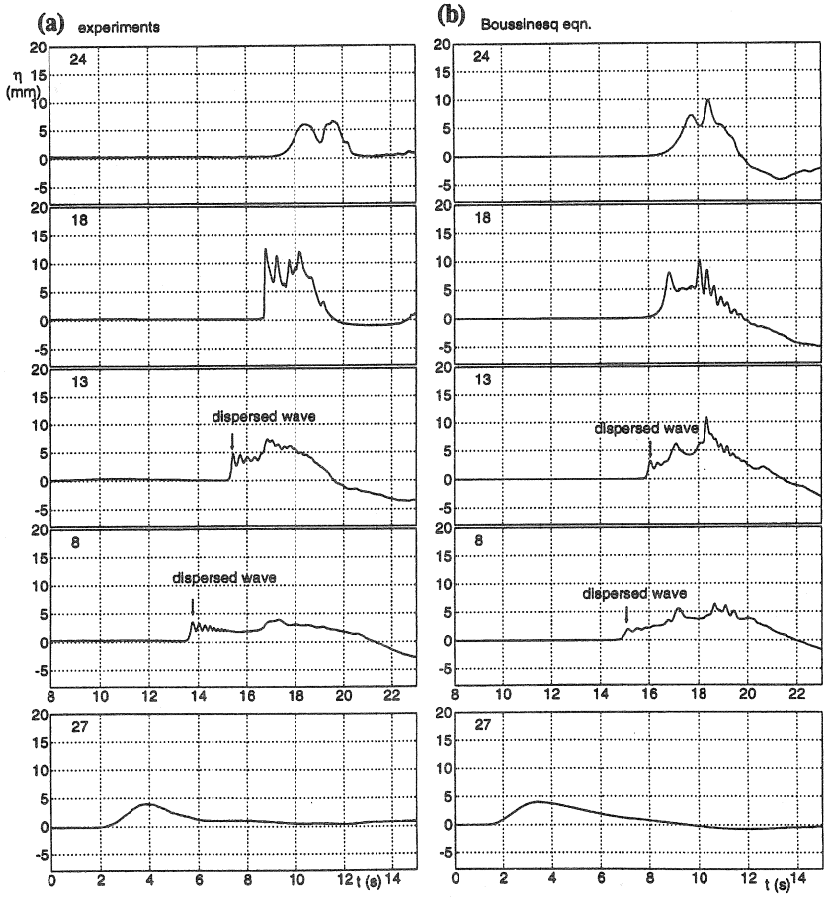

FIG. 9. Comparisons of Surface Elevations: (a) Experimental Data; (b) Numerical Predictions. (Number at Upper Left Corner Indicates Wave Gauge Locations Shown in Fig. 7; Numerical Model Simulates Wave Dispersion but Tends to Underestimate Dispersed Wave Height)

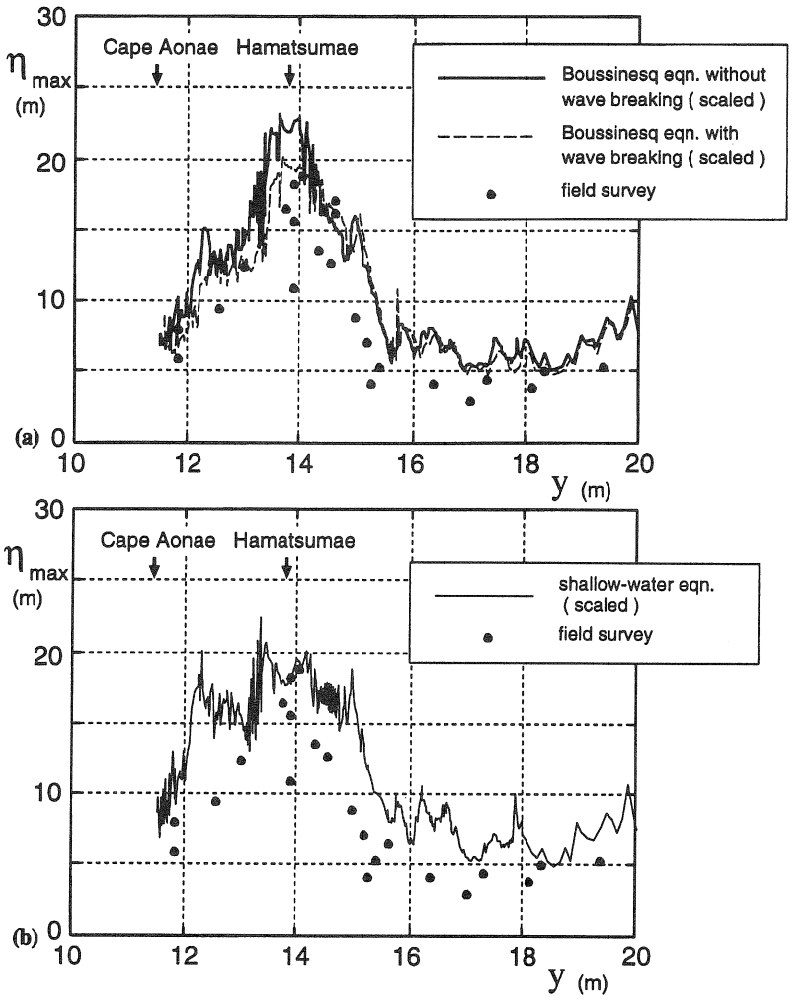

FIG. 10. Distributions of Maximum Surface Elevations Along Coastline (Solid Line Shows Computation without Wave Breaking; Broken Line shows Computation with Wave Breaking)

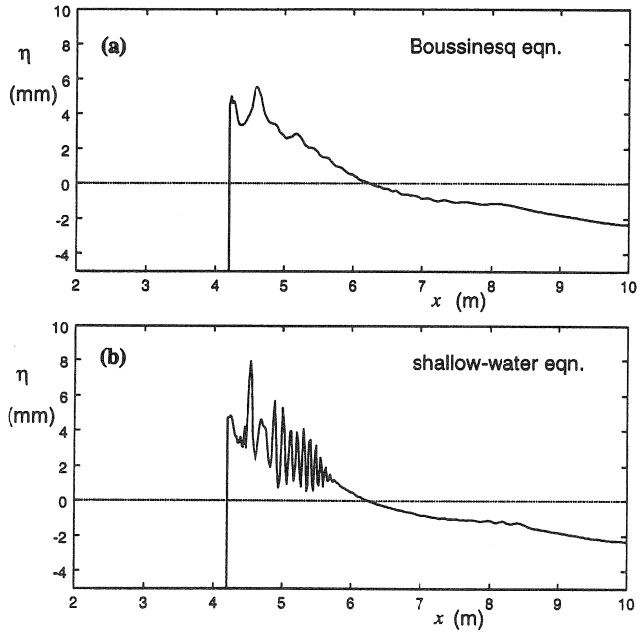

FIG. 11. Predicted Spatial Water-Surface Profiles along Line of $y = 12.5$ m at $t = 17$ s (See Fig. 7 for Profile Transection)

merical results in the range $15 < y < 20$ tend to overestimate the filed data, which suggests that the incident wave height used in the model was slightly large. The magnification rate of the inundation height at Hamatsumae to those in the nearby area are better predicted by the Boussinesq equation than by the shallow-water equation, indicating that the wave dispersion effect was essential in the estimation of tsunami height around Hamatsumae. Inclusion of the wave breaking effect tends to decrease the wave height in the area between Cape Aonae and Hamatsumae. However, it is difficult to confirm the significance of the wave breaking effect in tsunami simulation from the comparison of maximum surface elevations in this area. The overestimation of the shallow-water theory in the nearby Hamatsumae area was due to the numerical instability at the wave front. The instability was developed when the wave front entered a very shallow sea around Hamatsumae. Fig. 11 shows the spatial distribution of water-surface elevations along $y = 12.5$ m at $t = 17$ s. Fig. 11(a) shows the computation by the Boussinesq theory and Fig. 11(b) shows the computation by the shallow-water equation. Wave breaking is not involved in the computations. The large fluctuation noticed in the result by the shallow-water equation is considered to be responsible for the apparent large η_{max} in the nearby Hamatsumae area. No instability is noticed in the result by the Boussinesq theory.

CONCLUSIONS

A numerical model was presented for tsunami propagation, including the effects of dispersion and breaking of wave front. The numerical model was confirmed with the existing laboratory data of dispersive wave trains breaking on a slope. The model was applied to the propagation of the Southwest Hokkaido Earthquake tsunami around the southern part of Okushiri Island and compared with physical model tests. It was con-

firmed that the model could simulate the dispersion and breaking of the tsunami front and that the dispersion of waves resulted in the increase of tsunami height at Hamatsumae. The enhancement of runup at Hamatsumae are explained by the following two mechanisms: (1) tsunami focusing behind Murotsu Shoal due to refraction; and (2) the dispersion of the shoaled tsunami, which creates a series of dispersed waves riding on the base tsunami. The inclusion of wave breaking tended to suppress the dispersion of the wave front due to the mixing caused by wave breaking.

Further study is required on the formulation of eddy viscosity for complex bottom topographies.

ACKNOWLEDGMENTS

The writer wishes to express his sincere thanks to Shigenobu Tanaka and Kenji Noguchi, Public Works Research Institute, for fruitful discussions on the draft of this paper. Critical review by Harry Yeh, University of Washington, is also appreciated.

APPENDIX. REFERENCES

Goto, C. (1984). "Numerical study of Japan Sea tsunami in north Akita coast." *Proc., 31st Japanese Conf. on Coast. Engrg.*, Japan Soc. of Civil Engrs. (JSCE), Tokyo, Japan, 233–236 (in Japanese).

Hokkaido Tsunami Survey Group. (1993). "Tsunami devastates Japanese coastal region, Eos." *Trans. AGU*, 74(37), 417, 432.

Kato, K., and Tsuji, Y. (1994). "Estimation of fault parameters of the 1993 Hokkaido-Nansei-Oki earthquake and tsunami characteristics." *Bull. Earthquake Res. Inst.*, Univ. of Tokyo, Japan, 69, 39–66 (in Japanese).

Maa, J. P.-Y. (1990). "An efficient horizontal two-dimensional hydrodynamic model." *Coast. Engrg.*, 14, 1–18.

Noguchi, K., Sato, S., and Tanaka, S. (1995). "Propagation of Hokkaido Nansei-Oki earthquake tsunami around Cape Aonae." *Coast. Engrg. in Japan*, Tokyo, Japan, 38(2), 133–142.

Sato, S., and Kabiling, M. B. (1994). "A numerical simulation of beach evolution based on a nonlinear dispersive wave-current model." *Proc., 24th Conf. on Coast. Engrg.*, ASCE, New York, N.Y., 2557–2570.

Shuto, N. (1985). "The Nihonkai-Chubu earthquake tsunami on the north Akita coast." *Coast. Engrg. in Japan*, 28, Tokyo, Japan, 255–264.

Shuto, N., Matsutomi, H., and Ubana, M. (1994). "Characteristics of the Southwest Hokkaido earthquake tsunami and remaining problems." *Proc., Coast. Engrg.*, Japan Soc. of Civ. Engrs. (JSCE), Tokyo, Japan, 41, 236–240 (in Japanese).

Takahashi, T., Shuto, N., Imamura, F., and Matsutomi, H. (1994). "The measured and computed Hokkaido Nansei-oki earthquake tsunami of 1993." *Proc., 24th Conf. on Coast. Engrg.*, ASCE, New York, N.Y., 886–900.

Tsuruya, H., Nakano, S., and Ichinohe, H. (1984). "Experimental study on the deformation and run-up of tsunami in shallow water—case study of the tsunami caused by 1983 Nihonkai Chubu Earthquake." *Proc., 31st Japanese Conf. on Coast. Engrg.*, Japan Soc. of Civ. Engrs. (JSCE), Tokyo, Japan, 237–241 (in Japanese).

Watanabe, A., and Dibajnia, M. (1988). "A numerical model of wave deformation in surf zone." *Proc., 21st Conf. on Coast. Engrg.*, ASCE, New York, N.Y., 578–587.

Watanabe, A., Hara, T., and Horikawa, K. (1984). "Study on wave breaking condition for compound wave trains." *Coast. Engrg. in Japan*, Tokyo, Japan, 27, 71–82.

Yamashita, T., Takabayashi, T., and Tsuchiya, Y. (1994). "Numerical simulation of tsunami inundation caused by Southwest Hokkaido Earthquake." *Proc., Coast. Engrg.*, Japan Soc. of Civ. Engrs. (JSCE), 41, 231–235 (in Japanese).